Temperature-dependent optical spectroscopy studies of $Nd_{1-x}TiO_3$

J. Yang,[1,*] J. Hwang,[1] T. Timusk,[1,2] A. S. Sefat,[3] and J. E. Greedan[3]
[1]*Department of Physics and Astronomy, McMaster University, Hamilton, Ontario, Canada L8S 4M1*
[2]*The Canadian Institute of Advanced Research, Toronto, Ontario, Canada M5G 1ZB*
[3]*Department of Chemistry and Brockhouse Institute for Material Research, McMaster University, Hamilton, Ontario, Canada L8S 4M1*

(Received 27 February 2006; revised manuscript received 27 April 2006; published 31 May 2006)

The temperature dependent optical spectra are investigated in a well-characterized titanate system, $Nd_{1-x}TiO_3$, between 50 and 40 000 cm^{-1} at three different doping levels, $x=0.019$, 0.046, and 0.095, corresponding to a Mott-Hubbard insulator, a semiconductor and a correlated metal, respectively. Mid-gap states develop inside the Hubbard gap with hole doping. Based on the room-temperature spectra of the optical conductivity, the evolution rate of the excitations below 1.2 eV with doping is dependent on the electron correlation strength (U/W) of the parent insulator, which has been observed in other titanates as well. In the metallic sample ($x=0.095$), an anomalous enhancement of spectral weight below 1 eV develops with decreasing temperature. The partial spectral weight shows a quadratic dependence on temperatures up to the plasma frequency. Meanwhile, the metallic sample displays a Fermi-liquid behavior at low frequencies.

DOI: 10.1103/PhysRevB.73.195125 PACS number(s): 74.25.Gz

I. INTRODUCTION

The discovery of high-T_c superconductivity in cuprates[1] has led to increased interest in the transition metal oxides, and intensive experimental and theoretical studies have been done on these systems. Metal-insulator transitions, induced by compositional variations, are universal features in transition metal oxides.[2] In the Hubbard model,[3–5] two parameters play important roles in the metal-insulator transitions: The electron correlation strength U/W and the band filling n (the number of d electron per transition-metal cation site). Here, we use the optical conductivity as a probe to study the effect of band filling on the electronic properties of a perovskite-type $Nd_{1-x}TiO_3$ system. We start from the parent compound $NdTiO_3$ and introduce a concentration of x vacancies on the Nd^{3+} sites. Therefore, the band filling n per Ti site is $1-3x$, and equivalently, the hole concentration per Ti site is $3x$. By varying x from 0 to 1/3, we control the degree of electron filling of the d band on Ti^{3+}, n, from 1 ($NdTiO_3$) to 0 ($Nd_{2/3}TiO_3$). In the previous optical study by Arima *et al.*,[6] $NdTiO_3$ ($3d^1$) was considered to be a Mott-Hubbard (MH) insulator, where the charge gap is determined by the energy difference between the Coulomb-split Hubbard bands. On the other hand, the other end compound, $Nd_{2/3}TiO_3$, has no d electrons and is a charge-transfer insulator with a d-p characterized gap determined by the filled O $2p$ valence band and Ti $3d$ conduction band. Two metal-insulator-transitions are expected at two doping levels, $x\sim0.08$ and 0.24.[7,8] In this paper, we focus on the transition at the lower doping level.

We use infrared spectroscopy at various temperatures to investigate the variation of the transport properties of the $Nd_{1-x}TiO_3$ system at three doping levels ($x=0.019$, 0.046, and 0.095), across the low-doping-level metal-insulator transition. We address two main issues here regarding the optical properties of this titanate system. The first is the evolution of the low-lying states with hole doping. A comparison with the optical conductivity spectra of cuprate superconductors will be presented. The presence of mid-infrared absorption bands in $Nd_{1-x}TiO_3$ suggest that as the hole doping proceeds, mid-gap states develop inside the Hubbard gap in accordance with a two-component model of conductivity discussed in the cuprates.[9] Furthermore, we will quantitatively analyze the evolution rate of the optical excitations below 1.2 eV with doping. In the second part of this paper, we will focus on the interesting temperature-dependent features of the correlated metallic sample with $x=0.095$, a composition close to the metal-insulator transitions. The optical conductivity shows that an anomalous enhancement of spectral weight below 1 eV develops with decreasing temperatures. The partial spectral weight increases quadratically with decreasing temperatures. The dynamic mean field theory (DMFT) predicts such behavior in correlated metals. Finally, we find that the metallic sample exhibits a quadratic temperature and frequency dependence of the scattering rate in the low-frequency limit, characteristic of Fermi-liquid behavior.

II. EXPERIMENTS

A. Sample preparation and characterization

The microtwinned single crystals were grown in two different ways. The parent compound was grown using the floating-zone method. The doped samples of composition $x\sim0.046$ and 0.095 were made by a modified Bridgeman process.[8] To characterize the Nd concentration of the grown samples, neutron activation analysis was used with an estimated uncertainty of ±0.02. A very slight deviation of x from zero in the parent compound was found with $x=0.019(6)$. The other two doped samples were found to have $x=0.046(10)$ and $x=0.095(8)$, respectively. Four-probe resistivity measurements, shown in Fig. 1, and magnetic susceptibility measurements, indicated that the $x=0.019$ sample is an insulator, while the $x=0.046$ shows semiconductor behavior and they have antiferromagnetic to paramagnetic transitions, at around 90 K and 68 K, respectively.[8,10] No magnetic transitions were found in the metallic sample

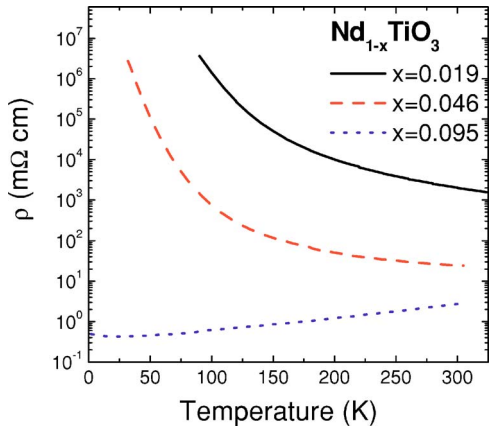

FIG. 1. (Color online) dc resistivity data of $x=0.019$, 0.046, and 0.095 of $Nd_{1-x}TiO_3$ obtained from four-probe resistivity measurements (Ref. 8).

($x=0.095$). The structure of $Nd_{1-x}TiO_3$ is perovskite with an orthorhombic distortion, the so-called $GeFeO_3$ type, which has been previously seen in a series of titanates.[11]

B. Optical measurements

The optical experiments were performed on well-polished surfaces, approximately 2×2 mm^2 in size, with a Bruker IFS 66v/s Fourier transform spectrometer in a ^{4}He flow cryostat. The nearly normal-incident reflectance of the sample was measured between 50 and 40 000 cm^{-1} at six different temperatures, from 28 K to room temperature. An *in situ* evaporation technique[12] was applied to correct geometrical effects of an irregular surface. We estimate the absolute accuracy of the reflectance to be better than ±0.5%. For Kramers-Kronig (KK) analysis, which was used to extract the optical constants, i.e., the real and imaginary parts of the optical conductivity, we need to extend the reflectance data beyond the frequency region actually measured in our study. For the metallic sample ($x=0.095$), the low-frequency reflectance was extrapolated toward zero frequency through the use of the Hagen-Rubens approximation, $1-R(\omega)\propto\sqrt{\omega}$, fitted to the lowest-frequency measured reflectance data. For the two insulating samples, we used the dc resistivity data[8] for the low-frequency extrapolation. At high frequencies, we employed the reflectance data of $BaTiO_3$ (Ref. 13) between 40 000 and 100 000 cm^{-1} for all three samples, and assumed a free carrier response, $R\propto\omega^{-4}$, beyond 100 000 cm^{-1}. The adoption of the data of $BaTiO_3$ is reasonable, since there is little difference among the reflectance of different titanates in the near-infrared region,[14] and a small shift of high-frequency reflectance will not substantially affect the optical conductivity spectra below 10 000 cm^{-1}.

III. HOLE-DOPING DEPENDENT OPTICAL PROPERTIES

A. Reflectance and optical conductivity

In Fig. 2(a), we present the room-temperature reflectance of the samples studied at the three doping levels, up to the highest frequency of our study. The semiconductor and the insulator show three sharp optical phonons in the far-infrared region of the spectra; characteristic of cubic perovskites. The small splitting of the second phonon band, as seen in the insulating sample, originates from the orthorhombic distortion of the cubic structure.[15] The phonon modes are much weaker in reflectance in the metallic sample. Through KK transformation of the reflectance, we obtained the real part of the optical conductivity at room temperature at the three doping levels, as shown in Fig. 2(b). The spectrum of the insulator consists of two separate electronic-absorption processes, a lower-frequency band with an onset at about 10 000 cm^{-1}, and a higher-frequency one starting at 30 000 cm^{-1}. The spectral weight of the low-frequency plateau between 10 000 and 30 000 cm^{-1} has been assigned to the MH transition between the lower Hubbard (LH) and upper Hubbard bands, and the rapid increase of spectral weight above 30 000 cm^{-1} to the charge-transfer (CT) transition from the filled O $2p$ states to the LH $3d$ band.[6] From the intersection point of the extrapolated linear fit to the band edge and the abscissa, we estimated the onsets of the two transitions to be ~0.8 eV and ~4 eV, respectively, consistent with previous studies.[6,16] (The remenant spectral weight below 0.8 eV is due to a slight Nd nonstoichiometry, $x=0.019$ as shown by neutron observation.[8]) The relative position of the two gap excitations suggests that the insulat-

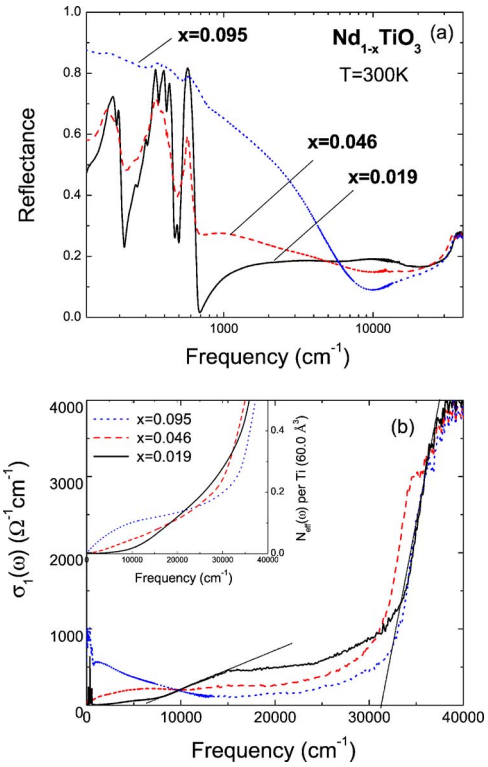

FIG. 2. (Color online) (a) The reflectance of $Nd_{1-x}TiO_3$ at three doping levels at room temperature. The $x=0.095$ sample shows metallic behavior, while $x=0.046$ and 0.019 have the optical spectra of a semiconductor and an insulator, respectively. (b) The corresponding optical conductivity of the three samples at room temperature. Dashed lines show the linear extrapolation of the edge of the transitions. The inset shows the partial sum rule for the three doping levels.

ing d^1 (Ti^{3+}) compound is a MH-type insulator rather than a CT insulator in the Zaanen-Sawatsky-Allen scheme.[17]

As we doped more holes into the system, the spectral weight of the MH transition decreased; whereas that inside the Mott gap increased monotonically, as seen in the doped samples in Fig. 2(b). The excitations inside the gap can be divided into two clear components; a sharp Drude absorption peak, which appears in the metallic sample, and a broad mid-infrared (MIR) absorption, with a spectral weight that increases with doping. The spectral weight of the MIR band moves to lower frequency with doping. Similar behavior has been seen in the $R_{1-x}Ca_xTiO_3$ system.[16]

B. Analysis and discussion

The transfer of spectral weight from the high-frequency region to the low-frequency part with doping is a general feature of strongly correlated systems.[18] However, it is interesting to note that in the Na_xCoO_2 system, no spectral weight transfer was found from the high-energy band transitions to the Drude component as the hole concentration is increased.[19] The doping-dependent low-frequency conductivity of $Nd_{1-x}TiO_3$ resembles that of the cuprate superconductor $La_{2-x}Sr_xCuO_4$ (LSCO) (Ref. 20) with a MIR absorption that grows and moves to lower frequencies with hole doping. Another similarity is that an isosbestic point, where conductivity curves cross, is present in both systems. The spectral weight lost above this point, ~1.2 eV in $Nd_{1-x}TiO_3$, moves to the region below it resulting in an overall conservation of spectral weight at 3 eV, where all three curves intersect as shown in the inset of Fig. 2(b). In this figure, the effective electron number $N_{\text{eff}}(\omega)$ was obtained from the integration, $N_{\text{eff}}(\omega)=2m_0V_{\text{Ti}}/(\pi e^2)\int_0^{\omega}\sigma_1(\omega')d\omega'$, where m_0 is the mass of an electron, $V_{\text{Ti}}=65.3$ Å^3 is the volume per Ti atom, e is the charge of an electron, and σ_1 is the optical conductivity. It should be noted that in LSCO, the MIR peak evolves into the Drude component above a certain doping level, and the CT gap excitation persists in the metallic samples. However, in titanates, the conductivity spectra related to the Hubbard gap excitations are quite weak at high doping levels, and the MIR peak is still present in the sample with the highest doping level of our study.

In the context of a two-component model, the above features in the optical conductivity spectra lead to some interesting consequences for the electronic structure of hole-doped $Nd_{1-x}TiO_3$. We assigned the MIR absorption in Fig. 2(b) to transitions from the LH band to the mid-gap state, which grows with doping inside the Hubbard gap, above E_F. The growth of the new mid-gap states with hole doping explains why the spectral weight of the MIR is growing with doping in the optical conductivity spectra. If we assign the Drude peak in the metallic sample to the quasi-particle spectral weight at E_F in the LH band, the proposed electronic structure is consistent with the existing photoemission or inverse photoemission data for hole-doped titanium oxides.[21–23] What is different from the other titanates here is that in the metallic phase of $Nd_{1-x}TiO_3$, the mid-gap state does not occupy the whole Hubbard gap and there remains a small gap above the Fermi surface. We can see the small gap

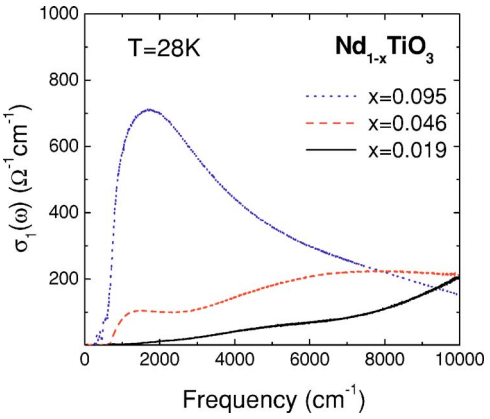

FIG. 3. (Color online) Expanded view of the lowest charge gaps at 28 K at different doping levels. To display the evolution of the mid-gap state clearly, we removed Drude and phonon contributions from the metallic sample and the phonons from the semiconductor and insulator.

in our optical spectra more clearly if we subtract the phonon and Drude contribution from the conductivity of $Nd_{0.905}TiO_3$ at the lowest temperature of our study as shown in Fig. 3. The figure shows the lowest charge gaps in the three samples, and we estimate the small gap in the metallic and the semiconducting samples to be about 0.057 eV and 0.087 eV in size, respectively. We expect that the small gap will vanish at higher doping levels and the top of the LH band and the bottom of the mid-gap band will coalesce.

Although the origin of the formation of the mid-gap state is not clear at this point, we can quantitatively analyze the rate of evolution of the excitations inside the Mott gap, or the rate of the spectral weight transfer with doping. Here, we adopted the procedure from an earlier study[16] and present our results in Fig. 4 in terms of the effective electron number $N_D=N_{\text{eff}}(\omega_c)_p-N_{\text{eff}}(\omega_c)_{p=0}$, associated with the Drude excitation and the MIR absorptions below the isosbestic point

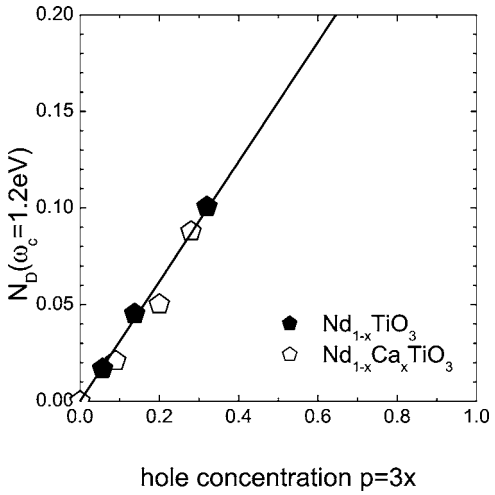

FIG. 4. Effective electron number related to the Drude and MIR excitations as a function of hole concentration p. The closed pentagons are our results of $Nd_{1-x}TiO_3$ and the open ones are for $Nd_{1-x}Ca_xTiO_3$ from previous studies (Ref. 16). The straight line is a least-squares fit to our data.

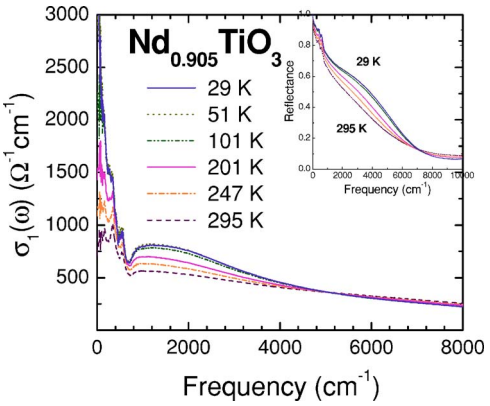

FIG. 5. (Color online) Reflectance (inset) and optical conductivity of the metallic sample $Nd_{0.905}TiO_3$ at different temperatures between 28 K and room temperature. Note the overall gain of spectral weight with temperature.

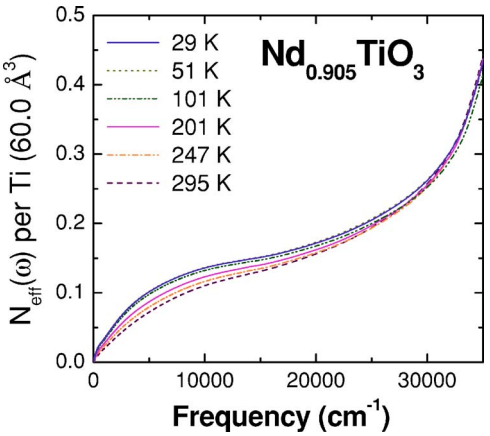

FIG. 6. (Color online) The partial spectral weight up to 35 000 cm^{-1} of $Nd_{0.905}TiO_3$ at different temperatures. The volume per Ti atom is $V_{Ti}=60.0$ Å^3.

($\omega_c \sim 1.2$ eV) plotted as a function of the doping levels (p). Here N_D represents the spectral weight transferred from the spectrum above ω_c to that below ω_c. Figure 4 shows that N_D increases approximately linearly with hole doping with a slope of $N_D/p=0.37$. The quantity N_D/p is called the spectral weight transfer rate. Previous spectroscopic studies[16] yielded a transfer rate of 0.31 ± 0.07 for the $Nd_{1-x}Ca_xTiO_3$ system. Within the systematic uncertainties of our study, the two systems have consistent transfer rate. Note that these two systems also have the same parent compound $NdTiO_3$. According to the studies by Katsufuji *et al.*[16] the rate of spectral weight transfer with doping of various series of titanate is a linear function of the electron correlation strength (U/W) of the corresponding parent insulator. Our optical study of the current titanate system confirms this conclusion.

IV. TEMPERATURE DEPENDENT OPTICAL PROPERTIES

A. Optical conductivity

In Fig. 5, we show the results of temperature-dependent measurements on our metallic sample $Nd_{0.905}TiO_3$. The low-frequency region of the optical conductivity includes a narrow Drude absorption peak, coexisting with three phonon peaks, and a broad MIR absorption. Notice that the spectral weight up to 5000 cm^{-1} increases monotonically with decreasing temperatures. The extra spectral weight at low temperatures has been transferred from the region above 5000 cm^{-1}, since the partial spectral weight is temperature independent above 32 500 cm^{-1}, as seen in Fig. 6, although the 101 K curve appears to deviate from this trend.

Ortolani *et al.*[24] showed, in a recent article, that the temperature dependence of the partial spectral weight $W(\Omega)$,

$$W(\Omega,T) \simeq W_0 - B(\Omega)T^2, \tag{1}$$

holds for conventional metals, such as gold, as well as for high-T_c superconductors, i.e., $Bi_2Sr_2CaCu_2O_{8+y}$ and LSCO. The partial spectral weight is a model-independent quantity defined as

$$W(\Omega,T) = \int_0^{\Omega} \sigma_1(\omega,T)d\omega. \tag{2}$$

We also verified Eq. (1) for $Nd_{0.905}TiO_3$ as shown in Fig. 7. It should be noted that the choice of high-frequency extrapolation can cause an additional uncertainty in the conductivity data above 10 000 cm^{-1} and in Fig. 7, the data at frequencies above 10 000 cm^{-1} have larger uncertainties than the rest. For clarity, all data have been normalized to make the intercept on ordinate axis unity. $W(T)/W_0$ at different cutoff frequencies (Ω) decays linearly with T^2 and the slope of each linear fit, B/W_0, is Ω dependent. Figure 8 displays the behavior of $B(\Omega)$ as a function of frequency, which describes the "thermal response" of carriers.[24] The peak around 5000 cm^{-1} is related to the intersection of the conductivity curves in Fig. 5, and B decreases with frequency above 5000 cm^{-1}. The behavior of B as a function of frequency is

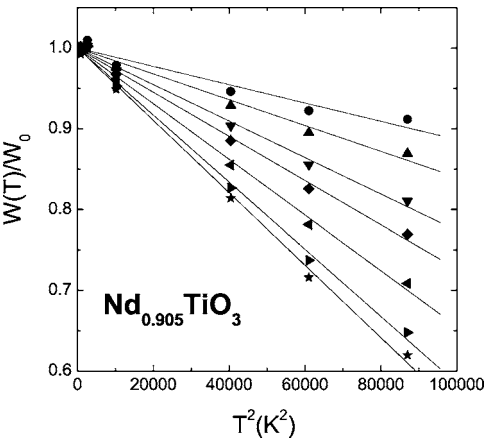

FIG. 7. Normalized temperature dependence of the spectral weight with different cutoff frequencies in $Nd_{0.905}TiO_3$. The symbols from top to bottom represent cutoffs of 20 000 cm^{-1}, 15 000 cm^{-1}, 10 000 cm^{-1}, 7500 cm^{-1}, 5000 cm^{-1}, 3000 cm^{-1}, and 2000 cm^{-1}, respectively. The straight lines are least-squares fits to the data.

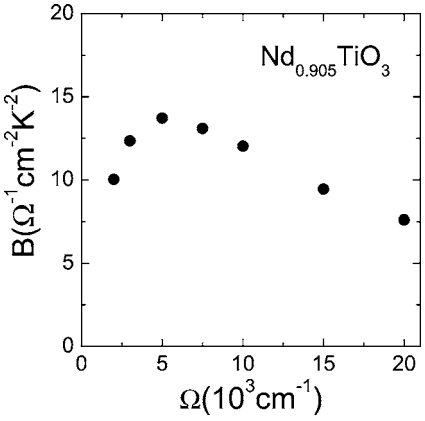

FIG. 8. The behavior of coefficient B as a function of frequency in $Nd_{0.905}TiO_3$.

different from that in both gold and LSCO. In Fig. 2 of the report by Ortolani *et al.*,[24] all T dependence in B for gold is below the plasma frequency (ω_p=20 500 cm^{-1}) and $B(\omega_p)=0$; while for LSCO, the value of B at $\omega_p \simeq 6800$ cm^{-1} is nonzero, 1.7 Ω^{-1} cm^{-2} K^{-2}. In our study for $Nd_{0.905}TiO_3$, the value of B at $\omega_p \sim 15\,000$ cm^{-1} is 10 Ω^{-1} cm^{-2} K^{-2}, much larger than the value for LSCO.

In the model of two components, we use a Drude oscillator for the free carriers and Lorentz oscillators to describe the MIR optical conductivity. The phonons are also modeled with oscillators. Table I shows the resulting parameters of the Drude oscillators and the phonons. The MIR region shows a hump around 1200 cm^{-1} at all temperatures, and a small gap forms right before the hump in Fig. 3 making an oscillator fit with a single Lorentzian to a high frequency, i.e., 5000 cm^{-1}, difficult. According to the Drude parameters, the temperature dependence of the scattering rate is consistent with the behavior of free charge carriers. However, the increase of the Drude spectral weight with decreasing temperature is contrary to the expectation that the number of free carriers should be constant as the temperature is varied. Moreover, even without the fitting parameters of the MIR absorptions, it is clear (in Fig. 5) that there is an anomalous enhancement of spectral weight with decreasing temperature between 600 to 5000 cm^{-1} in the optical conductivity.

A very similar anomalous enhancement of spectral weight was found for the paramagnetic phase of $CeTiO_{3.04}$ and the metallic phase of V_2O_3. Both systems show enhanced low-frequency spectral weight as the temperature is decreased.[25,26] Rozenberg *et al.*[26] treated the Hubbard model in DMFT, and predicted an enhancement of both Drude and midinfrared spectral weight as T is lowered for the correlated metallic states (in good agreement with the experimental results for V_2O_3). We observe the exact same anomalous shift of spectral weight to the Drude peak and the MIR band at 2000 cm^{-1} in our metallic sample.

These unusual shifts of spectral weight should be distinguished from the downward shift *within* the Drude band caused by narrowing of the Drude peak and the upward shift typically seen when a gap forms such as the spin-density-wave gap in electron doped cuprates.[27,28]

The temperature-dependence of the optical conductivity data of the semiconducting sample is also interesting. As seen in Fig. 9, the spectra below 10 000 cm^{-1} contain three main features. A fairly broad Drude peak grows with increasing temperature and can be barely seen at the lowest temperatures. In the intermediate-frequency range, two separated peaks appear at the lowest temperature, with different temperature dependencies. As the temperature is raised, the first peak broadens and finally almost disappears at room temperature. However, the second, higher-frequency peak, remains at high temperatures; moving to lower frequencies with increasing temperatures. The first peak could be assigned to small polarons,[29] but with an intermediate coupling since the frequency of the polaron is only twice the characteristic phonon frequencies of this system. The broadening of the first peak could also be the consequence of an increasing overlap with the second peak.

TABLE I. Parameters of Drude-Lorentz fits at different temperatures for the metallic sample $Nd_{0.905}TiO_3$. For the fits, ϵ_∞=4.80. $\omega_{p,D}$ and Γ_D are the plasma frequency and scattering rate of the Drude mode and ω_k, $\omega_{p,k}$, and Γ_k are center frequency, strength, and width of the kth Lorentz oscillator.

		295 K	247 K	201 K	101 K	51 K	29 K
Drude	$\omega_{p,D}$	5440	5900	6300	6700	6750	6750
(cm^{-1})	Γ_D	550	480	430	320	300	300
	$\omega_{p,1}$	515	500	500	300	300	200
	ω_1	165	165	165	160	159	159
	Γ_1	35	35	35	16	16	12
Phonons	$\omega_{p,2}$	1150	1060	1100	1170	1250	1150
(cm^{-1})	ω_2	337	345	345	345	345	345
	Γ_2	80	70	65	80	80	80
	$\omega_{p,3}$	1100	1160	1200	1300	1400	1300
	ω_3	550	555	555	555	555	555
	Γ_3	110	115	110	120	110	110

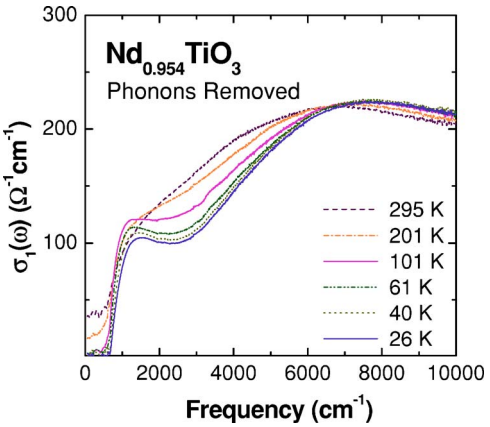

FIG. 9. (Color online) The optical conductivity of the semiconducting sample $Nd_{0.954}TiO_3$ at different temperatures between 28 K and room temperature.

B. Fermi-liquid behavior

The extended Drude model[30] provides an alternative way to the Drude-Lorentz analysis to study the non-Drude optical conductivity of $Nd_{0.905}TiO_3$. In this model, a single low-frequency Drude contribution is used with a frequency-dependent scattering rate and effective mass. The usual Drude expression for the conductivity now becomes

$$\sigma(\omega,T)=\frac{1}{4\pi}\frac{\omega_p^2}{1/\tau(\omega,T)-i\omega[1+\lambda(\omega,T)]} \tag{3}$$

where $\sigma(\omega,T)$ is the complex optical conductivity, ω_p is the plasma frequency, $1/\tau(\omega)$ is the scattering rate, and $1+\lambda(\omega)=m^*(\omega)/m$ is the ratio of the effective mass to the bare electron mass. To get the imaginary part of σ, the value of ε_∞ must be known. To include the spectral weight below the charge transfer transition in σ, we used the value of ε_1 at 23 000 cm^{-1} as our estimate of ε_∞. The calculated frequency-dependent scattering rate of the metallic sample at various temperatures is shown in Fig. 10. To clearly illustrate the low-frequency part of the scattering rate spectrum, all the phonon contributions have been subtracted from the complex conductivity. Around 750 cm^{-1}, a peak appears at all temperatures, which corresponds to the interband contribution in the midinfrared region. Because the extended Drude formalism describes only the features of the itinerant charge carriers, the scattering rate above 750 cm^{-1} may be not real. Therefore, we will only focus on the low-frequency region of the scattering rate spectrum in the following analysis.

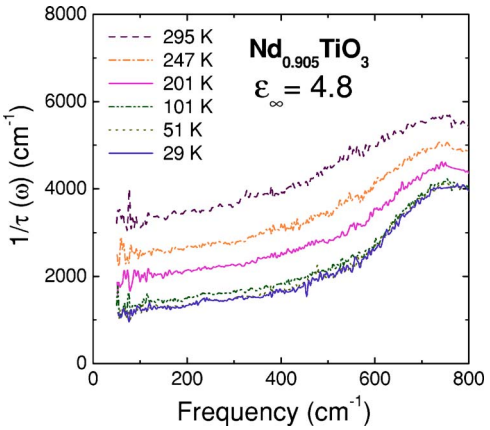

FIG. 10. (Color online) The frequency-dependent scatering rate at different temperatures for $Nd_{0.905}TiO_3$, obtained from the extended Drude model and ε_∞ was estimated to be 4.8.

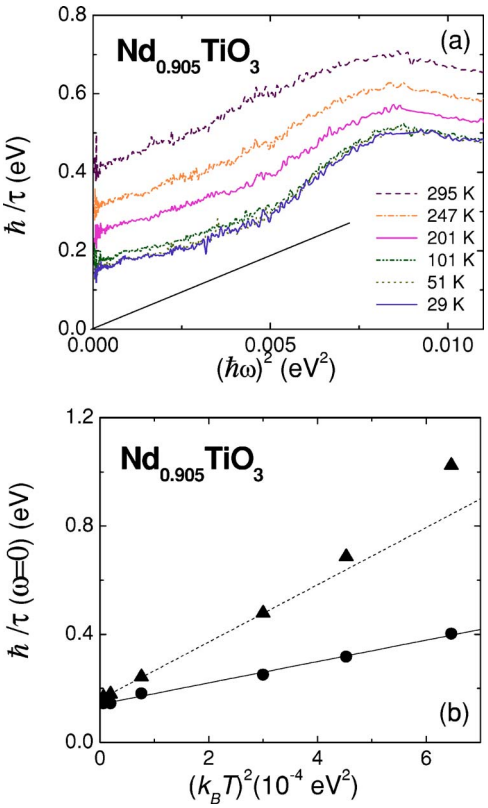

FIG. 11. (Color online) (a) Behavior of the scattering rate as a function of frequency squared at different temperatures. The solid line shows a least-squares fit to the room-temperature data. (b) Closed circles are the plot of the scattering rate at zero frequency vs temperature squared for $Nd_{0.905}TiO_3$. The solid line is a least-squares fit to the closed circles. The filled triangles represent the dc scattering rate derived from the dc resistivity data in Fig. 1. The straight line shows a least-squares fit to the data at low temperatures.

In Fig. 11(a), we plot the scattering rate spectra at various temperatures as a function of frequency squared. The curves seem to be parallel to each other, and we observed a nearly linear dependence on ω^2 at high temperatures below 0.1 eV, while the data at lower temperatures show certain deviation from the linear shape with the evidence of an onset of scattering at 0.07 eV (530 cm^{-1}). In the plot of the zero-frequency scattering rate versus temperature squared, as seen in Fig. 11(b), a linear dependence on T^2 is also present. It should be noted that there are discrepancies by a factor of 1.3–2 between the results of optical measurements and four-probe resistivity measurements. The difference may come from the contact geometry of the resistivity measurements. The two features, the temperature and the frequency dependence of the scattering rate, are consistent with the Fermi-

liquid theory,[31] according to the following equation:

$$\hbar/\tau(\omega,T) = \hbar/\tau_0 + \alpha(k_B T)^2 + \beta(\hbar\omega)^2, \quad (4)$$

where $\alpha/\beta = \pi^2 \simeq 9.87$. By least-square fits to the room-temperature curve in Fig. 11(a) and the optical data in Fig. 11(b), we estimate the coefficient of $(\hbar\omega)^2$ to be $\beta = 37.38\ \mathrm{eV}^{-1}$ and the coefficient of $(k_B T)^2$ to be $\alpha = 395.2\ \mathrm{eV}^{-1}$, respectively. As a result, α/β is 10.6 for $Nd_{0.905}TiO_3$ in our study, which is only 7% off the theoretical prediction. Consequently, considering the experimental errors in our study, the results for the correlated metal, $Nd_{0.905}TiO_3$, are consistent with the Fermi-liquid theory in the low-frequency limit. This kind of behavior has also been found previously in the paramagnetic metal $Ce_{0.95}Ca_{0.05}TiO_{3.04}$.[32]

V. CONCLUSIONS

In conclusion, we investigated the doping and temperature-dependent optical properties of the hole-doped Mott insulator $Nd_{1-x}TiO_3$. There are obvious differences between the titanate system and cuprate superconductors. This is not surprising since the cuprates are hole- or electron-doped CT insulators, and they have two-dimensional layer structures. We find that a so-called mid-gap state develops inside the Hubbard gap as the hole concentration increases in the current system. Meanwhile, the rate of spectral weight transfer with doping depends on the electron correlation strength of the parent insulator. Furthermore, for the correlated metallic sample ($x = 0.095$), the partial spectral weight is a linear function of T^2 and the sample shows a Fermi-liquid behavior in the low-frequency limit.

*Electronic address: yangj23@mcmaster.ca

[1] J. G. Bednorz and K. A. Müller, Z. Phys. B: Condens. Matter **64**, 189 (1986).
[2] M. Imada, A. Fujimori, and Y. Tokura, Rev. Mod. Phys. **70**, 1039 (1998).
[3] J. Hubbard, Proc. R. Soc. London, Ser. A **276**, 238 (1963).
[4] J. Hubbard, Proc. R. Soc. London, Ser. A **277**, 237 (1964).
[5] J. Hubbard, Proc. R. Soc. London, Ser. A **281**, 401 (1964).
[6] T. Arima, Y. Tokura, and J. B. Torrance, Phys. Rev. B **48**, 17006 (1993).
[7] G. A. Amow, N. P. Raju, and J. E. Greedan, J. Solid State Chem. **155**, 177 (2000).
[8] A. S. Sefat, G. M. Luke, M. N. Niewczas, J. D. Garret, H. Dabkowska, A. Dabkowski, and J. E. Greedan (unpublished).
[9] M. A. Quijada, D. B. Tanner, R. J. Kelley, M. Onellion, H. Berger, and G. Margaritondo, Phys. Rev. B **60**, 14917 (1999).
[10] A. S. Sefat, J. E. Greedan, and J. E. Cranswich (unpublished).
[11] D. A. McLean, Hok-Nam Ng, and J. E. Greedan, J. Solid State Chem. **30**, 35 (1979).
[12] C. C. Homes, M. A. Reedyk, D. A. Crandles, and T. Timusk, Appl. Opt. **32**, 2976 (1993).
[13] T. Kolodiazhnyi, J. Hwang, and T. Timusk (unpublished).
[14] D. A. Crandles, T. Timusk, J. D. Garrett, and J. E. Greedan, Physica C **201**, 407 (1992).
[15] D. A. Crandles, T. Timusk, J. D. Garrett, and J. E. Greedan, Phys. Rev. B **49**, 4299 (1994).
[16] T. Katsufuji, Y. Okimoto, and Y. Tokura, Phys. Rev. Lett. **75**, 3497 (1995).
[17] J. Zaanen, G. A. Sawatzky, and J. W. Allen, Phys. Rev. Lett. **55**, 418 (1985).
[18] H. Eskes, M. B. J. Meinders, and G. A. Sawatzky, Phys. Rev. Lett. **67**, 1035 (1991).
[19] J. Hwang, J. Yang, T. Timusk, and F. C. Chou, Phys. Rev. B **72**, 024549 (2005).
[20] S. Uchida, T. Ido, H. Takagi, T. Arima, Y. Tokura, and S. Tajima, Phys. Rev. B **43**, 7942 (1991).
[21] K. Morikawa, T. Mizokawa, A. Fujimori, Y. Taguchi, and Y. Tokura, Phys. Rev. B **54**, 8446 (1996).
[22] A. Fujimori, Jpn. J. Appl. Phys., Part 1 **7**, 125 (1992).
[23] S. W. Robey, V. E. Henrich, C. Eylem, and B. W. Eichhorn, Phys. Rev. B **52**, 2395 (1995).
[24] M. Ortolani, P. Calvani, and S. Lupi, Phys. Rev. Lett. **94**, 067002 (2005).
[25] T. Katsufuji and Y. Tokura, Phys. Rev. B **62**, 10797 (2000).
[26] M. J. Rozenberg, G. Kotliar, H. Kajueter, G. A. Thomas, D. H. Rapkine, J. M. Honig, and P. Metcalf, Phys. Rev. Lett. **75**, 105 (1995).
[27] Y. Onose, Y. Taguchi, K. Ishizaka, and Y. Tokura, Phys. Rev. B **69**, 024504 (2004).
[28] A. Zimmers, J. M. Tomczak, R. P. S. M. Lobo, N. Bontemps, C. P. Hill, M. C. Barr, Y. Dagan, R. L. Greene, A. J. Millis, and C. C. Homes, Europhys. Lett. **70**, 225 (2005).
[29] S. Fratini and S. Ciuchi, cond-mat/0512202 (unpublished).
[30] P. B. Allen, Phys. Rev. B **3**, 305 (1971).
[31] D. Pines and P. Nozieres, *The Theory of Quantum Liquids* (Benjamin, New York, 1966).
[32] T. Katsufuji and Y. Tokura, Phys. Rev. B **60**, 7673 (1999).